JOURNAL OF COMPUTATIONAL PHYSICS 121, 271–280 (1995)

An Adaptive Discrete-Velocity Model for the Shallow Water Equations

B. T. NADIGA

Theoretical Division and CNLS, Los Alamos National Laboratories, Los Alamos, New Mexico 87545

Received June 23, 1994; revised March 20, 1995

A new approach to solving the shallow water equations is presented. This involves using discrete velocities of an adaptive nature in a finite volume context. The origin of the discrete-velocity space and the magnitudes of the discrete-velocities are both spatially and temporally variable. The near-equilibrium flow method of Nadiga and Pullin is used to arrive at a robust second-order (in both space and time) scheme—the adaptive discrete velocity (ADV) scheme—which captures hydraulic jumps with no oscillations. The flow over a two-dimensional ridge, over a wide range of undisturbed upstream Froude numbers prove the robustness and accuracy of the scheme. A comparison of the interaction of two circular vortex patches in the presence of bottom topography as obtained by the ADV scheme and a semi-Lagrangian scheme more than validates the new scheme in two dimensions.

1. INTRODUCTION

As the name suggests, a discrete velocity gas is an ensemble of particles with each particle taking on one of a small finite set of allowable velocities [2–4]. Further, the interaction between particles is defined to achieve the desired macro-behavior of the system. The desired macro-behavior of the discrete-velocity gas could be a set of partial differential equations describing a particular physical phenomenon and which could itself have been derived either from the microscopics or written down as a phenomenological model. If the partial differential equations are derived from microscopics, the definition of the velocities and the interactions in the discrete-velocity gas system is in some sense a minimal representation of the microscopics of the original system. Such a discretization of the velocity space and definition of the particle interactions also form the basis for the lattice gas and lattice Boltzmann techniques which have been developed over the last eight years [5–7]. Mechanics of these models show that their strong point is the simple and elegant way in which they combine physics and numerics. In using these models to simulate fluid phenomena, however, the artifacts of the discretized velocity space [8] and its coupling to the physical lattice in the lattice gas and lattice Boltzmann techniques severly limit the operational window of these models. In view of the above two statements, we think that simple and yet very powerful schemes to solve partial differential equations can be arrived at by incorporating the discrete-velocity gas ideas in other more conventional numerical techniques. In this article we consider one such hybridization—the discrete-velocity gas with the finite volume technique—resulting in a scheme we call the adaptive discrete velocity (ADV) scheme.

The physical system we consider is the dynamics of the free surface in the long wave limit of an (shallow) incompressible and homogeneous layer of fluid. The set of partial differential equations that describe this system to the lowest order (in the shallowness parameter $\varepsilon = H/\lambda$, the ratio of the depth to the horizontal wavelength of interest) is the well-known classical shallow water equations and it is this set of partial differential equations that we seek to model.

In the next section, the shallow water equations are briefly discussed, followed by a brief description of the nine-velocity gas in Section 3. In Section 4, the adaptive nature of the discrete-velocities is introduced and the equivalence of the ADV model to the shallow water equations is shown. Section 5 gives a step by step numerical evolution of the ADV model on the lines of Nadiga and Pullin [1]. In Section 6 is a consideration of the asymptotic nature of the flow over a two-dimensional ridge [16], a computation with the ADV scheme of four representative cases whose asymptotic states are qualitatively different, and a detailed comparison of the results of the ADV scheme to the asymptotically exact values. In Section 7 is a two-dimensional example: the interaction of a pair of like-signed vortices in the presence of bottom topography. In this context, the results are compared to that obtained by an explicit two time level semi-Lagrangian scheme. We finally present a few conclusions.

2. THE SHALLOW WATER EQUATIONS

The classical shallow water equations are, in the presence of bottom topography,

$$\frac{\partial \eta}{\partial t} + \nabla \cdot \eta \mathbf{u} = 0,$$

0021-9991/95 $12.00

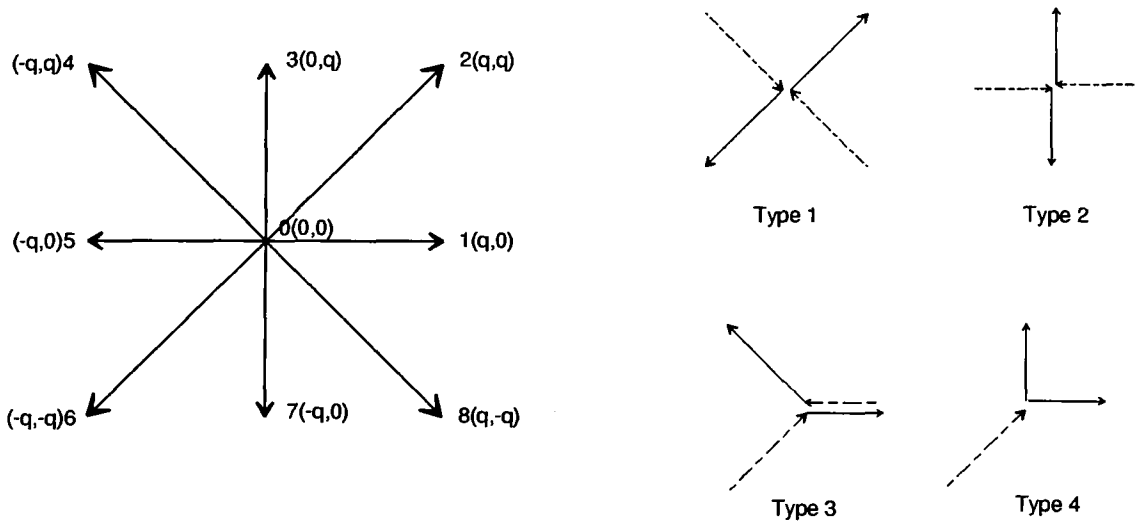

FIG. 1. The allowed velocities in the nine-velocity model are shown on the left side. The four types of mass, momentum, and energy conserving collisions are shown on the right. Collision type four involves particles whose precollision and postcollision speeds are different.

$$\frac{\partial \mathbf{u}}{\partial t} + \mathbf{u}\cdot\nabla\mathbf{u} = -g\nabla(\eta + b), \tag{1}$$

where η is the thickness of the fluid layer, b is the elevation of the bottom topography, $\mathbf{u}$ is the two-dimensional horizontal velocity, ∇ is the horizontal gradient operator (∂_x, ∂_y), and g is the acceleration due to gravity acting in the negative y-direction. $b + \eta$ gives the elevation of the free surface. Assuming that the viscous force exerted by the bottom is negligible, the above equations are derived from the Euler equations [9] under the hydrostatic approximation and describe the depth-independent fast dynamics of an incompressible layer of fluid. (Also called the barotropic mode in ocean dynamics.)

3. THE DISCRETE-VELOCITY MODEL

The discrete-velocity model we consider is the nine-velocity gas [11–13]. Figure 1 shows the allowed velocities ($\mathbf{q}_a$, $a = 0, \ldots, 8$)—four velocities each of speed q directed along the horizontal and vertical, speed $\sqrt{2}q$ along the diagonals, and a zero speed. Also shown are the four types of mass, momentum, and energy conserving collisions which serve to thermalise the distribution. The equilibrium relations representing detailed balancing of the collisions in the model, are

$$\begin{aligned} &n_0 n_2 = n_1 n_3, \quad n_0 n_4 = n_3 n_5, \quad n_0 n_6 = n_5 n_7, \\ &n_0 n_8 = n_7 n_1, \quad n_1 n_5 = n_3 n_7, \end{aligned} \tag{2}$$

where n_a is the probability of a particle having an allowable discrete-velocity $\mathbf{q}_a$. The mass, momentum, and total energy in terms of the population densities are

$$\begin{aligned} n &= n_0 + n_1 + n_2 + n_3 + n_4 + n_5 + n_6 + n_7 + n_8, \\ nu_x &= q(n_1 + n_2 - n_4 - n_5 - n_6 + n_8), \\ nu_y &= q(n_2 + n_3 + n_4 - n_6 - n_7 - n_8), \\ ne_t &= q^2(n_1 + n_3 + n_5 + n_7 + 2(n_2 + n_4 + n_6 + n_8)), \end{aligned} \tag{3}$$

where $e_t = \frac{1}{2}(u_x^2 + u_y^2) + e$. The equilibrium velocity distribution $\mathbf{n} = (n_a, a = 0, \ldots, 8)$ is obtained by the solution of above nine equations, Eq. (2) and Eq. (3). The stationary equilibrium distribution $(u_x = 0, u_y = 0)$, is simply

$$n_0 = n\left(1 - \frac{e}{q^2}\right)^2, \quad n_1 = \frac{n}{2}\left(1 - \frac{e}{q^2}\right)\frac{e}{q^2}, \quad n_2 = \frac{n}{4}\left(\frac{e}{q^2}\right)^2, \tag{4}$$

with $n_3 = n_5 = n_7 = n_1$ and $n_4 = n_6 = n_8 = n_2$.

4. THE EQUIVALENCE OF THE TWO SYSTEMS

To represent the shallow water equations as a discrete-velocity gas, we consider the nine-velocity gas discussed above under two simple transformations (see Fig. 2):

- The origin of the discrete-velocity space is translated to $\mathbf{u}(x, t)$, where $\mathbf{u}(x, t)$ is the temporally and spatially varying shallow water velocity field.
- The unit of discrete velocity, q is scaled so that the particle populations are all positive and $|\mathbf{u}| < q$.

For convenience, the shallow water equations, Eq. (1), are rewritten as

$$\frac{\partial \eta}{\partial t} + \nabla\cdot\eta\mathbf{u} = 0,$$

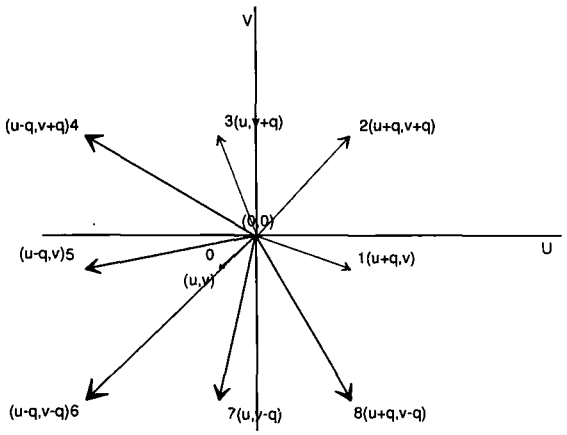

FIG. 2. The adaptive nine-velocity model. The origin of the discrete-velocity space and the unit of discrete-velocity q is determined by the local velocity $\mathbf{u} = (u, v)$ of the shallow water system.

$$\frac{\partial \eta \mathbf{u}}{\partial t} + \nabla \cdot \left(\eta \mathbf{u} \otimes \mathbf{u} + \frac{\eta^2}{2} \right) = -\eta \nabla b, \tag{5}$$

where $\otimes$ represents the binary outer product operator. The above equations have also been nondimensionalized using the undisturbed upstream depth η_u for the reference length and the undisturbed upstream long wavelength gravity wave speed $\sqrt{g\eta_u}$ for the reference velocity.

The two primary quantities in Eq. (5), the depth η and the horizontal velocity $\mathbf{u}$, are related to the local state of the discrete-velocity gas as follows:

a. As mentioned previously, the velocity $\mathbf{u}$ is used to translate the origin of the local discrete-velocity space (see Fig. 2), so that the allowed discrete-velocities now are $\mathbf{c}_a = \mathbf{u} + \mathbf{q}_a$, $a = 0, ..., 8$, and to scale the unit of velocity in that space so that the resulting particle populations are all positive and $|u| < q$ (along x-axis, and $|v| < q$ along y-axis): $q = \max(\alpha|u|, \sqrt{\eta/2})$ or $q = \max(\alpha|v|, \sqrt{\eta/2})$, α is 1.3 for flows with hydraulic jumps and 1.1 otherwise.

b. The density of the discrete-velocity gas n is set equal to the depth of the shallow layer of fluid η.

c. The discrete-velocity gas is assumed stationary with respect to the local origin, i.e., $u_x = u_y = 0$ in Eq. (3).

d. The internal energy ne of the discrete-velocity gas is set to the gravitational potential $\eta^2/2$.

Now considering the evolution of the discrete-velocity gas, the (model) Boltzmann equations [12]—a statement of the conservation of the number of particles with a particular discrete-velocity—are

$$\frac{\partial n_a}{\partial t} + \mathbf{c}_a \cdot \nabla n_a = Q_a(\mathbf{n}, \mathbf{n}), \quad a = 0, ..., 8, \tag{6}$$

where Q_a is the nonlinear collision operator and the left-hand side represents streaming of particles with velocity $\mathbf{c}_a$. The zeroth and first-order velocity moments of Eq. (6) give, respectively, noting that the moments of the collision terms on the right-hand side vanish owing to the mass and momentum conserving nature of each collision,

$$\begin{aligned} \frac{\partial n}{\partial t} + \nabla \cdot \overline{n_a \mathbf{c}_a} &= 0, \\ \frac{\partial \overline{n_a \mathbf{c}_a}}{\partial t} + \nabla \cdot \overline{n_a \mathbf{c}_a \otimes \mathbf{c}_a} &= 0, \end{aligned} \tag{7}$$

where the overbar denotes averaging with respect to the discrete-velocities. From a, b, c, d above and symmetry of the discrete-velocities,

$$\begin{aligned} \overline{n_a \mathbf{c}_a} &= \overline{n_a(\mathbf{u} + \mathbf{q}_a)} = \eta \mathbf{u}, \quad \text{since } \overline{n_a \mathbf{q}_a} = 0. \\ \overline{n_a \mathbf{c}_a \otimes \mathbf{c}_a} &= \overline{n_a(\mathbf{u} + \mathbf{q}_a) \otimes (\mathbf{u} + \mathbf{q}_a)} \\ &= n\mathbf{u} \otimes \mathbf{u} + \overline{n_a \mathbf{q}_a \otimes \mathbf{q}_a} \\ &= ne\mathbf{I} + \eta \mathbf{u} \otimes \mathbf{u} = \tfrac{1}{2}\eta^2 + \eta \mathbf{u} \otimes \mathbf{u}. \end{aligned}$$

Finally, if the bottom forcing in Eq. (5) is introduced as external forcing for the discrete-velocity gas, the equivalence is complete.

For convenience, the equations may be rewritten as

$$\frac{\partial \mathbf{f}}{\partial t} + (\nabla \cdot \mathbf{G})^{\mathrm{T}} = \mathbf{b}$$

with

$$\begin{aligned} \mathbf{f} &= \begin{pmatrix} \eta \\ \eta \mathbf{u} \end{pmatrix}, \quad \mathbf{b} = \begin{pmatrix} 0 \\ -\eta \nabla b \end{pmatrix}, \\ \mathbf{G} &= \left[\eta \mathbf{u}, \eta \mathbf{u} \otimes \mathbf{u} + \frac{\eta^2}{2} \right] = [\overline{n_a \mathbf{c}_a}, \overline{n_a \mathbf{c}_a \otimes \mathbf{c}_a}]. \end{aligned} \tag{8}$$

5. THE NUMERICAL TECHNIQUE

The standard discrete velocity models have served as useful models for computational fluid dynamics only in the *incompressible* or *slightly compressible* regimes, where the variations in the internal energy is small. It is for this reason—that only a very small range of internal energies have to be represented—that the standard discrete-velocity models use just one single speed. (In a recent work McNamara, Garcia, and Alder [19] use a 3D 21-velocity lattice-Boltzmann model to study the Rayleigh–Benard convection and they find that the maximum to minimum specific internal energy ratio that they can satisfactorily represent with the model is just 1.5.) If, however, a large range of internal energies have to be represented, a larger

number of speeds would have to be used and the propagation of population densities is no more computationally cheap: the larger the number of speeds and the more disparate the speeds, the more difficult it gets to propagate the densities. It is for this reason, that the flux-based evolution scheme for discrete-velocity gases was established in [1]. An additional advantage of this methodology is that while the number of fluxes to be calculated remains a constant with increasing number of velocities in a model, the number of densities to propagate increases as the number of velocities in the model. Also note that in [19], for reasons of stability, the *full* propagation of population densities had to be abandoned in favor of a more conventional Lax–Wendroff time-stepping procedure. In the present case, where the speed of the particles change continuously from point to point, full propagation of the densities is ruled out and the evolution is based on the flux calculating scheme of [1].

For simplicity, consider an uniform square tiling of the two-dimensional domain of interest, with each unit square representing a slab of the discrete-velocity gas. The values of the slab-averaged η and $\mathbf{u}$ are represented at the slab centroids. The evolution at each centroid proceeds as in the following steps:

Step 1. Use Eq. (4) to convert $\mathbf{f} = (\eta, \eta\mathbf{u})$ to n_0, n_1, and n_3: $q = \max(\alpha|u|, \sqrt{\eta/2})$,

$$n_0 = \eta\left(1 - \frac{\eta}{2q^2}\right)^2, \quad n_1 = \frac{\eta}{2}\left(1 - \frac{\eta}{2q^2}\right)\frac{\eta}{2q^2}, \quad n_2 = \frac{\eta}{4}\left(\frac{\eta}{2q^2}\right)^2. \tag{9}$$

Step 2. Calculate the split fluxes $\mathbf{G}^+$ and $\mathbf{G}^-$ using the definitions

$$\mathbf{G}^+ = \begin{pmatrix} \overline{n_d^{c_{ax}>0} c_{ax}} & \overline{n_d^{c_{ax}>0} c_{ax}^2} & \overline{n_d^{c_{ax}>0} c_{ay} c_{ax}} \\ \overline{n_d^{c_{ay}>0} c_{ay}} & \overline{n_d^{c_{ay}>0} c_{ax} c_{ay}} & \overline{n_d^{c_{ay}>0} c_{ay}^2} \end{pmatrix}, \quad \mathbf{G}^- = \begin{pmatrix} \overline{n_d^{c_{ax}<0} c_{ax}} & \overline{n_d^{c_{ax}<0} c_{ax}^2} & \overline{n_d^{c_{ax}<0} c_{ay} c_{ax}} \\ \overline{n_d^{c_{ay}<0} c_{ay}} & \overline{n_d^{c_{ay}<0} c_{ax} c_{ay}} & \overline{n_d^{c_{ay}<0} c_{ay}^2} \end{pmatrix}, \tag{10}$$

where $\overline{n_d^{c_{ax}>0} c_{ax}}$ is the average $\overline{n_d c_{ax}}$ taken only over the discrete velocities $\mathbf{c}_a$ which have a positive x-component c_{ax}, etc. For example, when $u > 0$ and $v > 0$,

$$\mathbf{G}^+ = \begin{pmatrix} uP + (u+q)Q & u^2P + (u+q)^2 & uvP + (u+q)vQ \\ vP + (v+q)Q & vuP + (v+q)uQ & v^2P + (v+q)^2Q \end{pmatrix},$$

$$\mathbf{G}^- = \begin{pmatrix} (u-q)Q & (u-q)^2Q & (u-q)vQ \\ (v-q)Q & (v-q)uQ & (v-q)^2Q \end{pmatrix},$$

where $P = (n_0 + 2n_1)$ and $Q = (n_1 + 2n_2)$.

Step 3. Assuming a linear distribution of the fluxes within the slabs, interpolate G_{11}^+, G_{12}^+, and G_{13}^+ to $(i + \frac{1}{2}, j)$, G_{21}^-, G_{22}^-, and G_{23}^- to $(i, j - \frac{1}{2})$, etc. and apply the minmod limiter to the interpolated fluxes:

$$\begin{aligned} G_{11}^+(i + \tfrac{1}{2}, j) &= G_{11}^+(i,j) + \tfrac{1}{2}\text{minmod}(\Delta_{\text{bck}} G_{11}^+(i,j), \Delta_{\text{fwd}} G_{11}^+(i,j)), \\ G_{21}^-(i, j - \tfrac{1}{2}) &= G_{21}^-(i,j) - \tfrac{1}{2}\text{minmod}(\Delta_{\text{bck}} G_{21}^-(i,j), \\ &\qquad \Delta_{\text{fwd}} G_{21}^-(i,j)), \text{ etc.}, \end{aligned} \tag{11}$$

where

$$\Delta_{\text{fwd}} G_{11}^+(i,j) = G_{11}^+(i+1,j) - G_{11}^+(i,j),$$
$$\Delta_{\text{bck}} G_{21}^-(i,j) = G_{21}^-(i,j) - G_{21}^-(i,j-1), \text{ etc.}$$

Minmod is the one-dimensional total-variation-diminishing operator as discussed in [14, 15],

$$\text{minmod}(p,q) = \text{sgn}(p)\begin{cases} 0 & \text{if } \text{sgn}(p) \neq \text{sgn}(q) \\ \min\{|p|, |q|\} & \text{if } \text{sgn}(p) = \text{sgn}(q), \end{cases}$$

with $\text{sgn}(p)$ being the sign of p and $|p|$ being the absolute value of p.

Step 4. Calculate $\mathbf{G}(\mathbf{i} + \frac{1}{2}) = \mathbf{G}^+(\mathbf{i} + \frac{1}{2}) + \mathbf{G}^-(\mathbf{i} + \frac{1}{2})$, where $(\mathbf{i} + \frac{1}{2}) = (i + \frac{1}{2}, j)$ and $(i, j + \frac{1}{2})$ in turn.

Step 5.

$$\mathbf{f}^{t_0 + \Delta t/2} = \mathbf{f}^{t_0} + \frac{\Delta t}{2}(\nabla \cdot \mathbf{G}^{t_0} - \eta^{t_0} \nabla b), \tag{12}$$

where, e.g.,

$$\nabla \cdot \begin{pmatrix} G_{11} \\ G_{21} \end{pmatrix} = \frac{G_{11}(i + \frac{1}{2}, j) - G_{11}(i - \frac{1}{2}, j)}{\Delta x} + \frac{G_{21}(i, j + \frac{1}{2}) - G_{21}(i, j - \frac{1}{2})}{\Delta y}.$$

Step 6. Repeat steps 1–4, using $\mathbf{f}^{t_0 + \Delta t/2}$ to obtain $\mathbf{G}^{t_0 + \Delta t/2}$, and take the full time step to obtain $\mathbf{f}^{t_1}$:

$$\mathbf{f}^{t_1} = \mathbf{f}^{t_0} + \Delta t(\nabla \cdot \mathbf{G}^{t_0 + \Delta t/2} - \eta^{t_0 + \Delta t/2} \nabla b). \tag{13}$$

In the above procedure the fluxes were interpolated and limited, instead, the primary quantities $\mathbf{f}$ could be interpolated

and limited. We have done both and the behavior of the two are essentially identical. Finally, we add that although the procedure to arrive at the final computational form may seem a bit complicated, the resulting code is extremely simple. (The code in CMFortran may be obtained from the author.)

6. FLOW OVER A 2D RIDGE

We consider the flow over a two-dimensional ridge as a test problem since (i) the exact asympotic solutions are known over a wide range of Froude numbers, (ii) they include both stationary and moving hydraulic jumps, and (iii) there are features of the flow which are extremely sensitive to artifacts of artificial and/or numerical viscosities. The two non-dimensional numbers, the upstream undisturbed Froude number $F_u = u/\sqrt{g\eta_u}$ and the nondimensional height of the mountain $b_c = b_{\max}/\eta_u$, where η_u is the depth of the undisturbed upstream fluid layer, are enough to prescribe a flow. The analytically determined flow characteristics as a function of these two parameters is shown in Fig. 3 (see Houghton and Kasahara [16]). In region I, the flow is everywhere subcritical and the free surface rises symmetrically about the crest of the ridge. In region III, the flow is everywhere supercritical and the free surface rises symmetrically about the obstacle. In region II, a hydraulic jump propagates upstream and a rarefaction downstream. While in region IIa, the hydraulic jump on the lee-side is stationary; it propagates downstream in region IIb. We consider the same four test cases as in [16] to sample the different regimes. The computational domain consists of 40.96

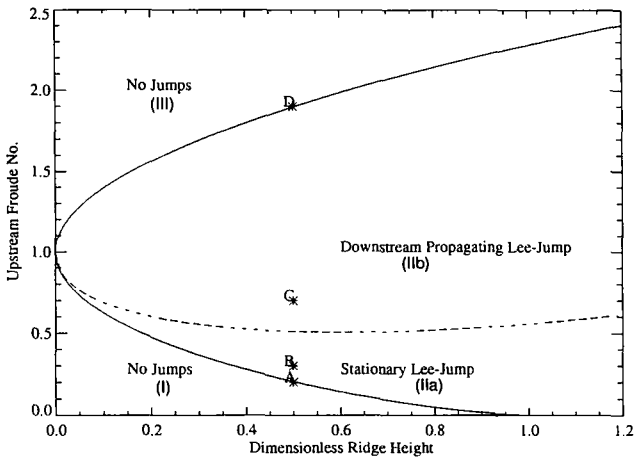

FIG. 3. The phase portrait for the shallow fluid flow over a two-dimensional ridge. The parameters b_c (dimensionless ridge height) and F_u (upstream Froude number) fully describe the flow. Associated with the lee-jumps are upstream propagating jumps and other downstream propagating rarefactions.

units of length $[-20.48, 20.48]$ in the horizontal, 1 unit being the undisturbed upstream depth of the fluid. Each unit is spanned by 100 points (so that $\Delta x = 0.01$) and the boundary condition is periodic. The central 20.48 units of the horizontal domain are shown. The time step is such that $(c_u)_{\max}\Delta t/\Delta x$ is between 0.8 and 1.0. The form of the mountain is $0.5b_c(1 + \cos(\pi|x|/L)$, where $L = 1.25$ is the half width of the ridge, and $0 \le |x| \le L$. The initial condition is a flat free surface at 1 and

TABLE I

Comparison of the ADV Scheme to Exact Asymptotic Values

Case item	A		B		C		D	
	Exact	ADV	Exact	ADV	Exact	ADV	Exact	ADV
η_A			1.0672	1.0672	1.3677	1.3677		
F_A			0.2338	0.2338	0.3579	0.3579		
C_l			−0.7503	−0.75	−0.5724	−0.5703		
η_c	0.3852	0.3855	0.3964	0.3963	0.6211	0.6209	1.4722	1.4723
F_c	0.5192	0.5187	0.6296	0.6296	0.7881	0.7888	1.2905	1.2905
C_r					0.1541	0.1543		
η_B					0.3298	0.3298		
F_B					1.4846	1.4845		
η			0.2339	0.2367				
F			1.0669	1.0543				
η_+			0.6221	0.6220				
F_+			0.4012	0.4053				
η_X			0.9603	0.9603	0.9281	0.9281		
F_X			0.2599	0.2599	0.6268	0.6271		

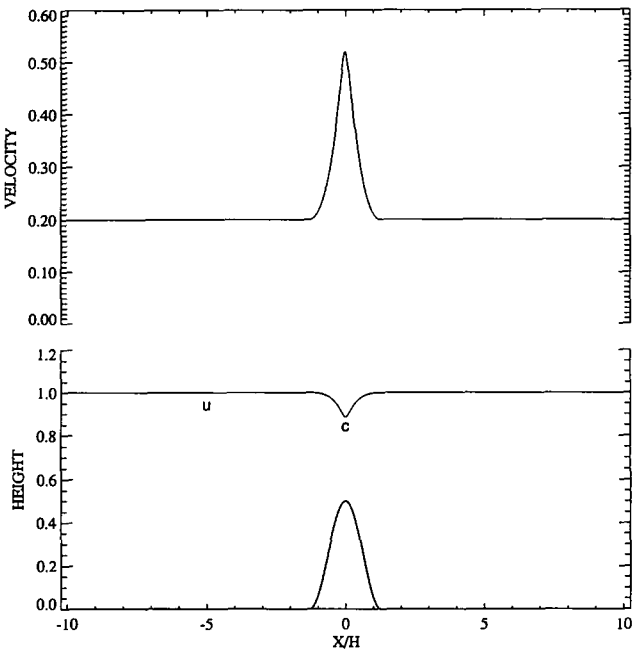

FIG. 4. Case A. Subcritical flow over a 2D ridge: $F_u = 0.2$; $b_c = 0.2$; $b_c = 0.5$; time = 20.48. The free surface dips symmetrically about the ridge.

uniform velocity F_u. The comparison of the numerical results to the exact asymptotic values is shown in Table I.

6.1. *Case A* ($F_u = 0.2$, $b_c = 0.5$)

This case corresponds to a fully subcritical flow with the free surface dipping symmetrically about the ridge. Figure 4 shows the numerical solution (u in the figure corresponds to an upstream location and c to the crest. These are the points at which comparisons are made to the exact values; see Table I).

6.2. *Case B* ($F_u = 0.3$, $b_c = 0.5$)

The main features of this case are an upstream propagating hydraulic jump, a stationary lee-side hydraulic jump, and a downstream propagating rarefaction. Figure 5 shows the numerical solution. (The upstream hydraulic jump has propagated outside the presentation window.) It is our experience with other numerical schemes that the region immediately downstream of the crest for this combination of parameters is the most difficult to handle numerically and is the most sensitive to numerical and/or artificial viscosity. Therefore, Fig. 6 magnifies this region. (The solid line is the same run as in Fig. 5.) The hydraulic jump is two cells wide, there are no oscillations, and the rising free surface downstream of the jump is clean.

In Fig. 6, we also compare the solution in Fig. 5 with the case where the resolution is cut down fourfold (and the time step is four times as large) but otherwise exactly the same setup. The degradation of the solution is faithful to the exact solution, with the degradation being confined to the vicinity of the hydraulic jump.

6.3. *Case C* ($F_u = 0.7$, $b_c = 0.5$)

The lee-side hydraulic jump in the present case propagates downstream. The overshoot of the free surface on the downstream side of the upstream-propagating hydraulic jump is suspected to be physical. (See Fig. 7.)

6.4. *Case D* ($F_u = 1.9$, $b_c = 0.5$)

The flow is everywhere supercritical and in the asymptotic state, the free surface rises symmetrically about the ridge. To eliminate the transients, the horizontal domain was extended by a factor of two, but the resolution was cut down by a factor of two ($\Delta x = 0.02$). The wave in the right half of the domain (downstream of the obstacle) is the transient. (See Fig. 8.)

The exact asymptotic behavior in all the cases above can be obtained as a solution of nonlinear algebraic equations resulting from the conservations and shock jump conditions [16]. The detailed comparisons of all the features of the flow to the exact asymptotic quantities are presented in Table I. The agreement is excellent. The errors are confined to the regions of the flow most sensitive to artifacts of the implicit artificial viscosity and even there they are about 1%.

7. AN EXAMPLE TWO-DIMENSIONAL CALCULATION

In this section, we consider the interaction between a pair of like-signed vortices in the presence of bottom topography.

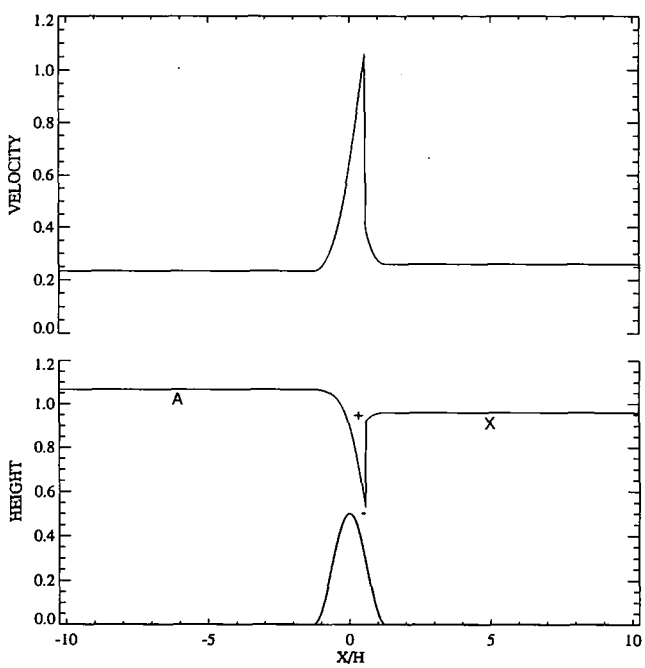

FIG. 5. Case B. Flow with stationary lee-side hydraulic jump: $F_u = 0.3$; $b_c = 0.5$; time = 20.48.

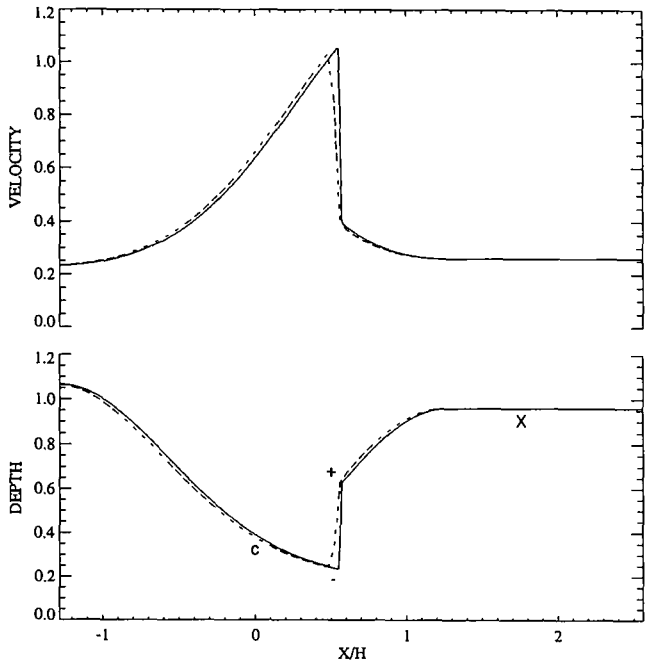

FIG. 6. Case B. Flow in the vicinity of the ridge: $F_u = 0.7$; $b_c = 0.5$; time = 20.48. The dot-dashed line is the result for the same case but with a fourfold reduced resolution and a consequent four times larger timestep.

The results of the ADV schemes are compared to that obtained by an explicit semi-Lagrangian solver.

7.1. *Restoring Boundaries*

In order to simulate this problem, periodic boundaries are unacceptable (for they would simulate an infinite train of vortex pairs). Further, there may be gravity waves generated by the vortex–vortex interaction, and so that these gravity waves do not in turn act on the vortices, we simulate absorbing boundaries. It consists of introducing a linearly varying restoring force which is nonzero outside the domain of physical interest in both the height and the momentum equations [18]:

$$\mathbf{r} = \frac{\mathbf{f}(\mathbf{x}) - \mathbf{f}_{\text{bnd}}(\mathbf{x})}{\tau(\mathbf{x})},$$

where

$$\tau = \begin{cases} \dfrac{r - r_{\text{bnd}}}{r_{\max} - r_{\text{bnd}}} \beta \Delta t, & \text{if } r > r_{\text{bnd}} \\ 0, & \text{otherwise.} \end{cases} \tag{14}$$

In the above formula, $\mathbf{f}_{\text{bnd}}(\mathbf{x})$ is the desired value to which $\mathbf{f}(\mathbf{x})$ is to be restored and $\beta\Delta t$ is the restoration time scale. With a computational domain of 1024 × 1024 slabs, we used the region $r > 480$ as the absorbing region with a restoration time of $10\Delta t$. The free surface elevation was restored to 1.0, the undisturbed height and the velocity was restored to (0, 0), the velocity at infinity.

7.2. *Interaction of a Pair of Vortices*

$$\mathbf{u} = \begin{cases} (-\omega(y - y_c), \omega(x - x_c)), & \text{if } r > a, \\ \left(-\omega \dfrac{a^2}{r^2}(y - y_c), \omega \dfrac{a^2}{r^2}(x - x_c)\right), & \text{if } r \le a, \end{cases}$$

$$\eta = \begin{cases} 1 - \omega^2 a^2 + \dfrac{\omega^2}{2} r^2, & \text{if } r > a, \\ 1 - \dfrac{\omega^2 a^4}{2r^2}, & \text{if } r \le a \end{cases} \tag{15}$$

is an exact vortex patch solution of Eq. (1). ω is the constant vorticity within the patch of radius a centered at (x_c, y_c), and r is the distance of a point (x, y) from (x_c, y_c).

The initial condition (in both the methods) consists of two vortex patches of the above form, with $\omega = 3.0$ and $a = 0.32$ (see Fig. 9). The center of the first patch is at (1.28, 1.28) and the center of the other patch is at (−1.28, −1.28). Centered at (0, 0) is an isolated right circular hill whose elevation is of the form $0.5b_c(1 + \cos(\pi r/L))$, $0 \le r \le L$, where $L = 1.92$ is the half width of the hill and $b_c = 0.5$ is the height of the crest. The simulation domain is a square form (−10.24, −10.24) to (10.24, 10.24), tiled by 1024 × 1024 slabs. The absorbing

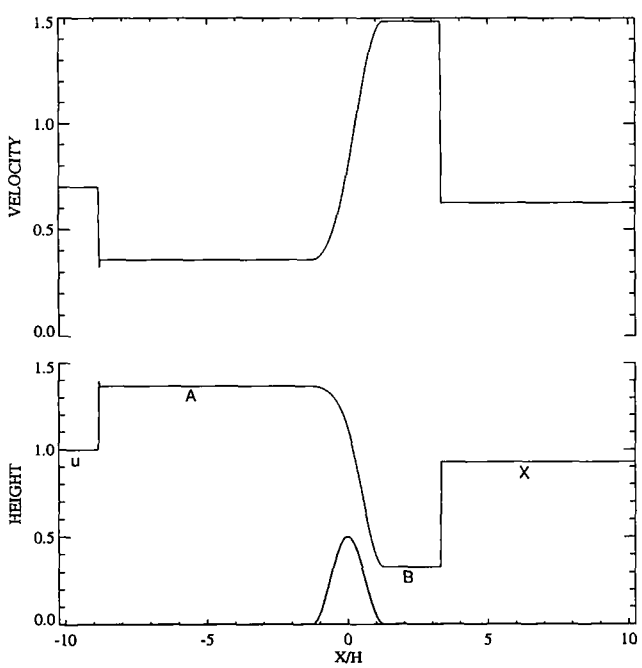

FIG. 7. Case C. Downstream propagating lee-side hydraulic jump: $F_u = 0.7$; $b_c = 0.5$; time = 15.36.

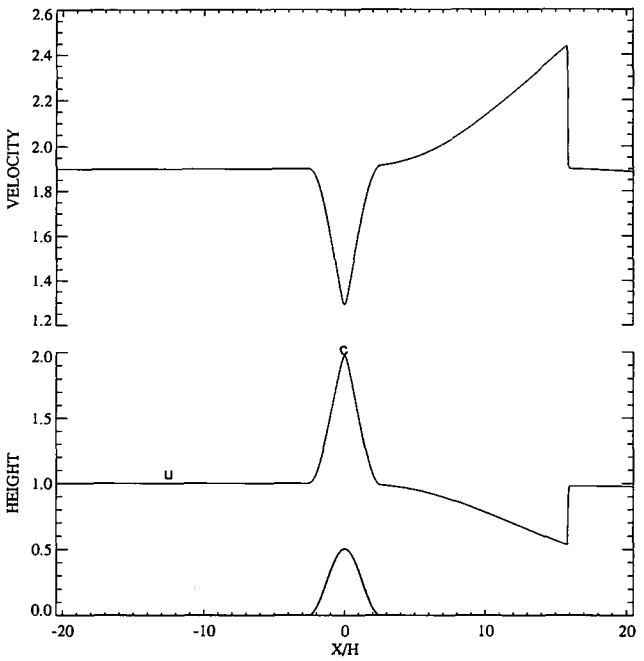

FIG. 8. Case D. Fully supercritical flow over a ridge: $F_n = 1.9$; $b_r = 0.5$; time = 10.24.

boundaries are in the region $r > 9.60$. The restoring time scale is $10\Delta t$.

The semi-Lagrangian scheme is an explicit two time level scheme and is second-order accurate in space and time [17]. It uses a flux-corrected monotone advection (interpolation) operator based on the second-order Trembeck scheme. It has to be noted that the monotonicity of the advection operator does not in any way ensure monotonicity of the free surface elevation and the velocities. The departure point calculations consist of a predictor and a corrector step, the height equation is solved using the flow Jacobian [17] and the absorber forces are treated implicitly in both the height and velocity equations.

Δt was 0.006 for the ADV scheme and 0.008 for the semi-Lagrangian scheme. The Eulerian CFL number defined as $\Delta t\,(|u|/\Delta x + |v|/\Delta y + \sqrt{\eta}\sqrt{1/\Delta x^2 + 1/\Delta y^2})$ is respectively 0.86 and 1.14. It is not our intent to make detailed comparisons of the relative efficiencies of the two schemes, but we report the relative computational costs of the two schemes for this particular problem: with a time step of 0.006 for the ADV scheme and 0.008 for the semi-Lagrangian scheme, the semi-Lagrangian scheme took about 60% longer than the ADV scheme on a 512 node CM5 partition, but it took only about 35% longer on a 128-node partition. This is explained by the more communication-intensive nature of the semi-Lagrangian scheme, even when there is no indirect addressing involved. So when the subgrid size—the number of grid points assigned to each processing unit—increases, as when a small number of processing units are used, the communication overhead decreases. In addition, the intricacies of programming the CM5 (in the data parallel mode) restrict the utility of these comparisons.

One of the attractive features of semi-Lagrangian schemes, however, is that the time step is not limited by the CFL criterion as with Eulerian schemes (already evident with the timestep of 0.008). Thus with the shallow water equations, the only restriction on the timestep in explicit semi-Lagrangian schemes is the resolution of the gravity waves. So, the semi-Lagrangian scheme was also run with a timestep of 0.012, which corresponded to a gravity wave based Courant number of 0.86 (an Eulerian CFL number of 1.73). With this timestep, however, (a) there is a communication overhead associated with indirect addressing resulting in an overall speedup of only about 9% over a timestep of 0.008 (at which no indirect addressing was necessitated) and (b) there is a reduction in accuracy. We therefore only present the semi-Lagrangian results for the timestep of 0.008.

Figure 10 shows a snapshot at time 32.76 using the ADV scheme, and Fig. 11 at the same time uses the semi-Lagrangian scheme. The overall evolution of the two vortices in the two schemes is almost identical. Plotted in Fig. 12 is the azimuthal velocity and free surface elevation profiles through a vertical cross section ($x = 0.48$), passing approximately through the center of the lower vortex in Fig. 10 and Fig. 11. While the correspondence outside of the core of the vortex is remarkably good; the core of the vortex is clearly smaller in the ADV

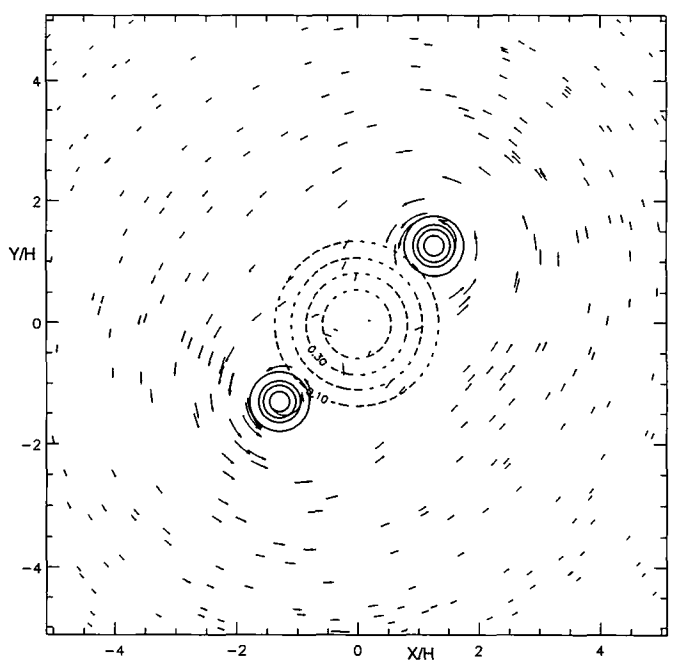

FIG. 9. The contour plot of the initial conditions for both the ADV scheme and the semi-Lagrangian scheme. The two vortex patches of the form of Eq. (15) are located symmetrically with respect to the right circular mountain centered at (0, 0). The contours of the mountain are shown in dot-dashed lines, the free surface elevation in solid lines and the arrows represent the velocity field.

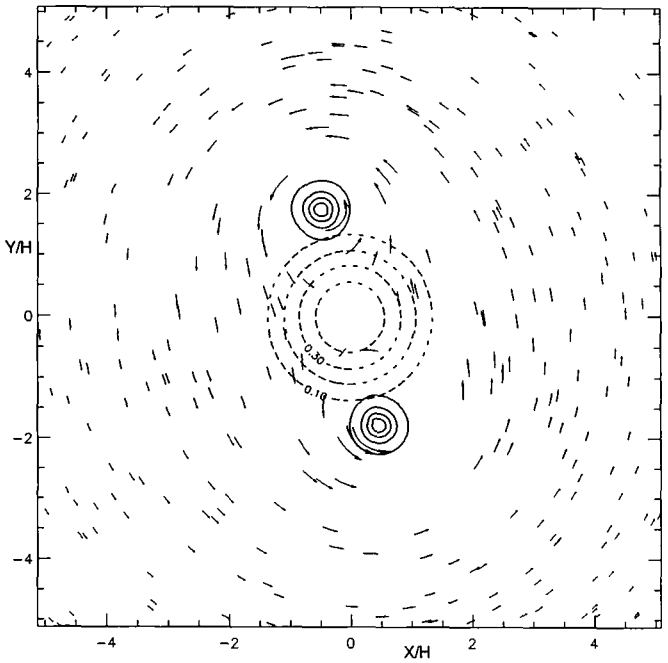

FIG. 10. The contour plot of the free surface elevation and the velocity field at time = 32.76, using the ADV scheme. The format of the plot is the same as in Fig. 9.

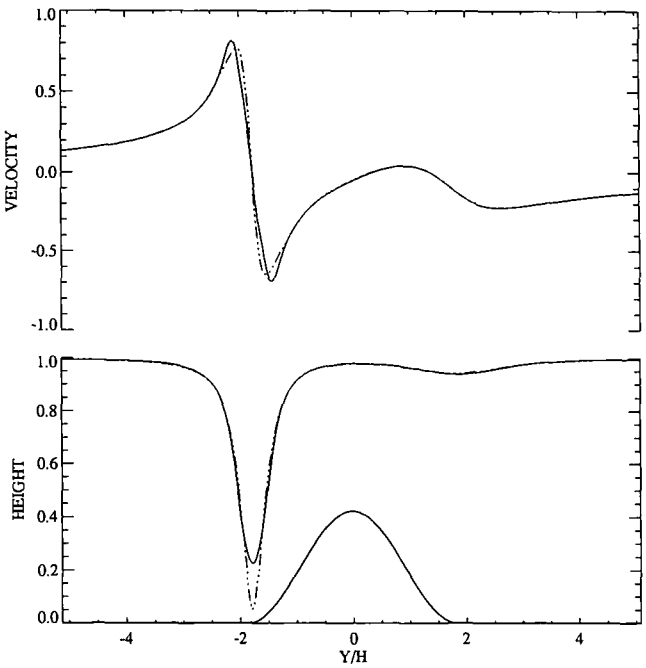

FIG. 12. A comparison of the free surface elevation and the azimuthal velocity profiles at time = 32.76, as obtained by the semi-Lagrangian scheme and the ADV scheme. The cross section approximately passes vertically through the center of the lower vortex patch. The solid line is the semi-Lagrangian result and the dot-dashed line the result from the ADV scheme.

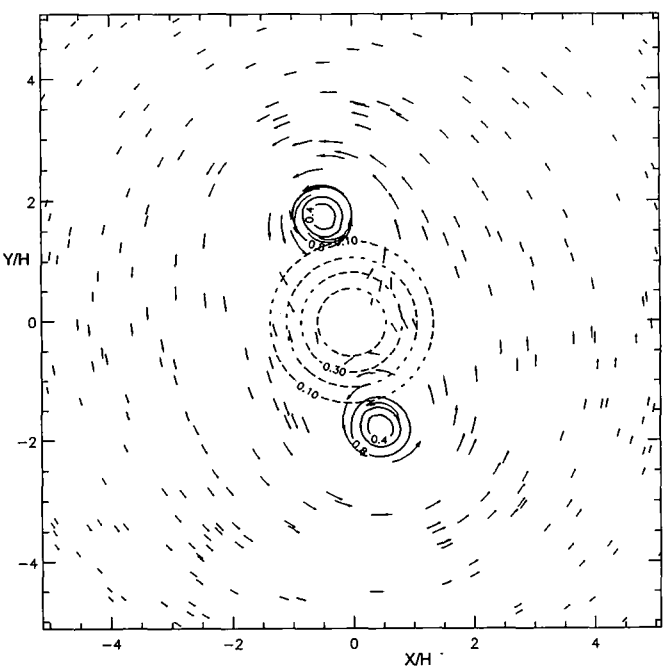

FIG. 11. The contour plot of the free surface elevation and the velocity field at time = 32.76, using the semi-Lagrangian scheme. The format of the plot is the same as in Fig. 9.

scheme as compared to the semi-Lagrangian scheme. This needs to be investigated further. It has also to be kept in mind that the semi-Lagrangian scheme, as it is used, cannot handle hydraulic jumps; an artificial viscosity (which has to be tuned appropriately for each particular case to avoid spurious oscillations) has to be added. Finally, the preservation of the physical symmetries of the problem verify the isotropy of the scheme despite the one-dimensional nature of the limiting procedure (Eq. (11)).

8. CONCLUSION

We have presented a new approach to solving the shallow-water equations based on discrete velocities. The resulting second-order (in space and time) scheme for the shallow water equations is very simple and yet robust; it can handle flows over a wide range of Froude numbers accurately and capture hydraulic jumps over 2–3 slab widths with no oscillations. The adaptive nature of the discrete-velocities (i.e., the floating reference and variable scaling of the discrete velocities) is a new paradigm of using these models in other numerical techniques and is expected to be of wider applicability than just the shallow water equations which were studied in this article.

ACKNOWLEDGMENTS

I thank Len Margolin and Piotr Smolarkiewicz for discussions on semi-Lagrangian techniques and other numerical issues; Darryl Holm, Len Margolin,

Piotr Smolarkiewicz, Roberto Camassa, and Wooyoung Choi (who also pointed out Eq. (15)) for discussions on shallow water; Shiyi Chen, Gary Doolen, and Guy Mcnamara for discussions on lattice Boltzmann methods; the Advanced Computing Lab for making available their computing resources; and Donna Spitzmiller for secretarial help. I also thank one of the referees for comments on the numerical approach. This work was supported in part by the DOE under the CHAMMP program.

REFERENCES

1. B. T. Nadiga and D. I. Pullin, *J. Comput. Phys.* **112,** 162 (1994).
2. J. E. Broadwell, *Phys. Fluids* **7,** 1243 (1964).
3. J. Hardy and Y. Pomeau, *J. Math. Phys.* **13,** 1042 (1972).
4. R. Gatignol, *Théorie Cinétique des Gaz à Répartition Discrète de Vitesses,* Lecture Notes in Physics, Vol. 36 (Springer-Verlag, Berlin, 1975).
5. S. Wolfram, *J. Statist. Phys.* **45,** 471 (1986).
6. G. D. Doolen (Ed.), *Lattice Gas Methods for PDE's, 1989* (Addison–Wesley, Reading, MA, 1989).
7. G. D. Doolen (Ed.), *Lattice Gas Methods for PDE's: Theory, Applications and Hardware* Physica D, Vol. 47 (North Holland, Amsterdam, 1991).
8. B. T. Nadiga, Ph.D. thesis, Caltech, 1992.
9. P. A. Thompson, *Compressible-Fluid Dynamics,* **518** (1988).
10. G. B. Whitham, *Linear and Nonlinear Waves* (Wiley-Interscience, New York, 1974).
11. D. d'Humières and P. Lallemand, *Helv. Phys. Acta* **59,** 1231 (1986).
12. B. T. Nadiga, J. E. Broadwell, and B. Sturtevant, "A Study of a Multispeed Cellular Automaton," in *Rarefied Gas Dynamics: Theoretical and Computational Techniques,* Progress in Astronautics and Aeronautics, Vol. 118 (AIAA, Washington, DC) (1989), p. 155.
13. S. Chen, M. Lee, K. H. Zhao, and G. D. Doolen, *Physica D* **37,** 42 (1989).
14. B. Van Leer, *J. Comput. Phys.* **32,** 101 (1979).
15. H. C. Yee, NASA-TM 101088, 1989 (unpublished).
16. D. D. Houghton and A. Kasahara, *Commun. Pure App. Math.* **21,** 1 (1968).
17. P. K. Smolarkiewicz and J. A. Pudykiewicz, *J. Atm. Sci.* **49,** 2082 (1992).
18. P. K. Smolarkiewicz, private communication, 1994.
19. G. R. McNamara, A. L. Garcia, and B. J. Alder, *J. Statist. Phys.,* 1995, to appear.